PNAS
www.pnas.org

Supplementary Information for

AP-3-dependent targeting of flippase ATP8A1 to lamellar bodies suppresses activation of YAP in alveolar epithelial type 2 cells.

Seunghyi Kook[1], Ping Wang[1], Shufang Meng[1], Christopher S. Jetter[1], Jennifer M.S. Sucre[1], John T. Benjamin[1], Jason J. Gokey[2], Hayley A. Hanby[3,4], Alexa Jaume[3], Laura Goetzl[5], Michael S. Marks[3,6], Susan H. Guttentag[1,*]

*Corresponding author: Susan Guttentag, MD, 11111 Doctor's Office Tower, 2200 Children's Way, Nashville, TN 37232
Email: susan.guttentag@vumc.org
ORCID identifier: https://orcid.org/0000-0003-4420-5879

This PDF file includes:

Figures S1 to S8
Tables S1 to S2
Legends for Movies SV1 to SV8
SI References

Other supplementary materials for this manuscript include the following:

Movies SV1 to SV8

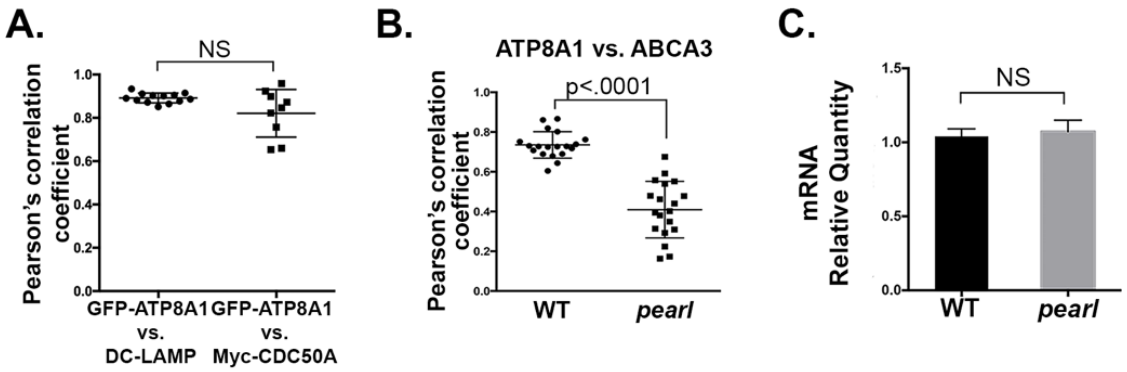

Figure S1:

A. Pearson's correlation coefficient acquired from images of transfected primary human AT2 cells in Figure 1B, comparing GFP-ATP8A1 with endogenous DC-LAMP and with exogenous Myc-tagged CDC50A (n=3 experiments; mean ± standard error).

B. Pearson's correlation coefficient acquired from images of primary mouse AT2 cells in Figure 1C, comparing endogenous ABCA3 and ATP8A1 (n=3 experiments; mean ± standard error).

C. RNA expression of *Atp8a1* in primary mouse AT2 cells. Quantitative RT-PCR for *Atp8a1* RNA from primary AT2 cells from WT and *pearl* mice (n=4; NS, not significant; mean ± standard error).

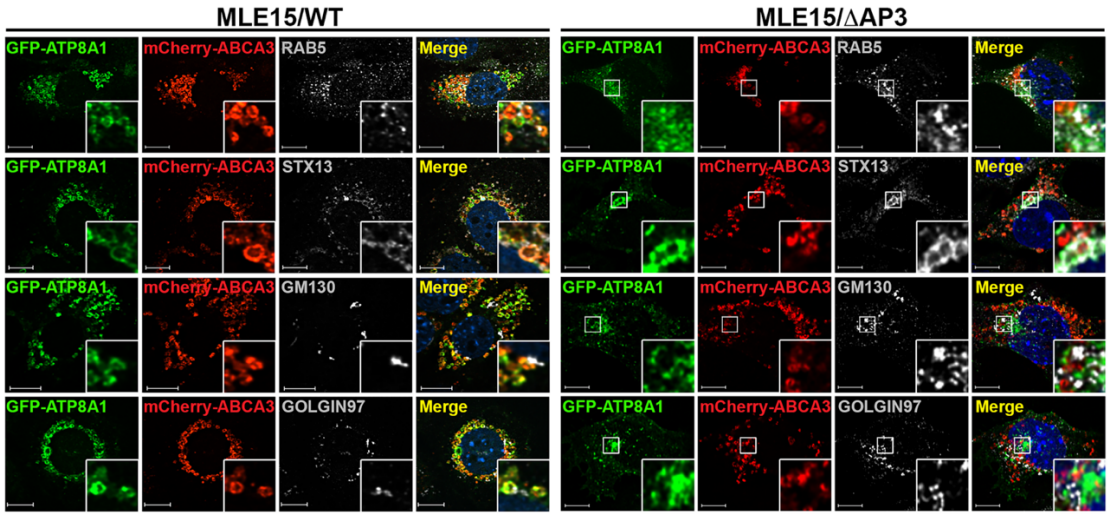

Figure S2: GFP-ATP8A1 localization to more proximal subcellular compartments in MLE15/WT and MLE15/ΔAP3 cells.

Representative confocal images of MLE15/WT and MLE15/ΔAP3 cells expressing exogenous GFP-ATP8A1 and mCherry-ABCA3, and immunostained for endogenous RAB5, STX13, GM130, and GOLGIN97 (scale bar = 10 microns).

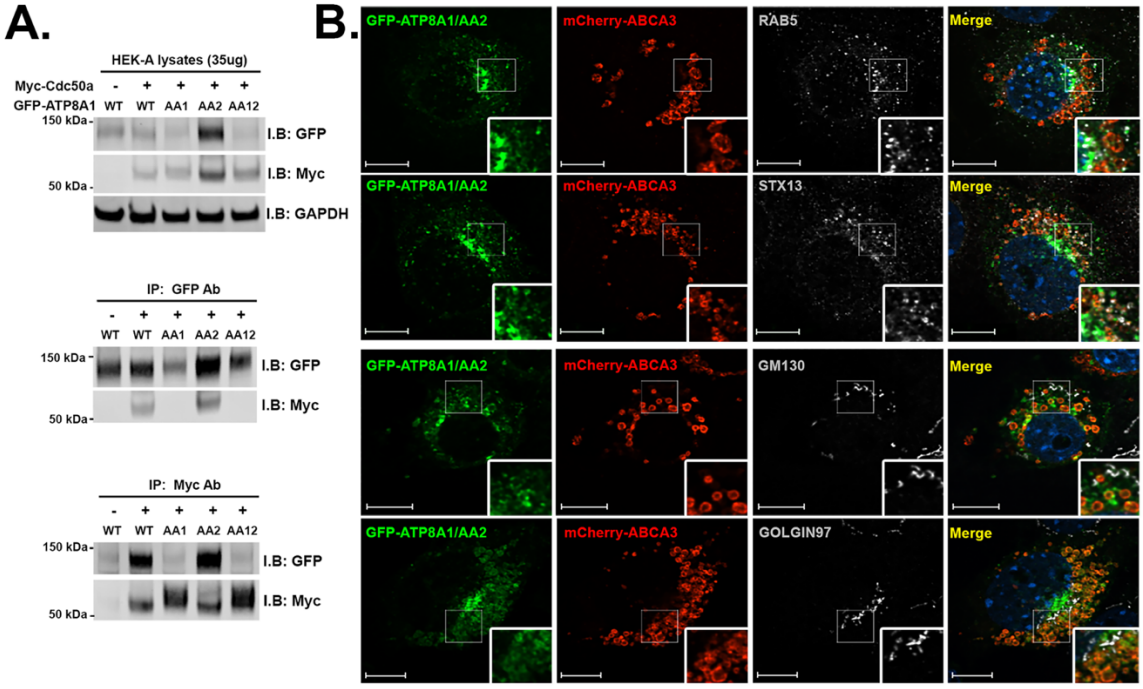

Figure S3: GFP-ATP8A1-AA2 localization to more proximal subcellular compartments in MLE15/WT cells.

A. Protein expression and coimmunoprecipitation of mutagenized GFP-ATP8A1 in HEK cells. Immunoblotting of HEK lysates (35 μg per lane) is shown using anti-GFP antibody or anti-Myc antibody in the upper panel. Co-immunoprecipitation utilizing anti-GFP (middle panel) or anti-Myc (bottom panel) was done using 500 μg of input lysate (representative of 2 experiments).

B. Representative confocal images of MLE15/WT cells expressing mCherry-ABCA3 and GFP-ATP8A1-AA2, with immunostaining for RAB5, STX13, GM130, and GOLGIN97 (scale bars = 10 microns).

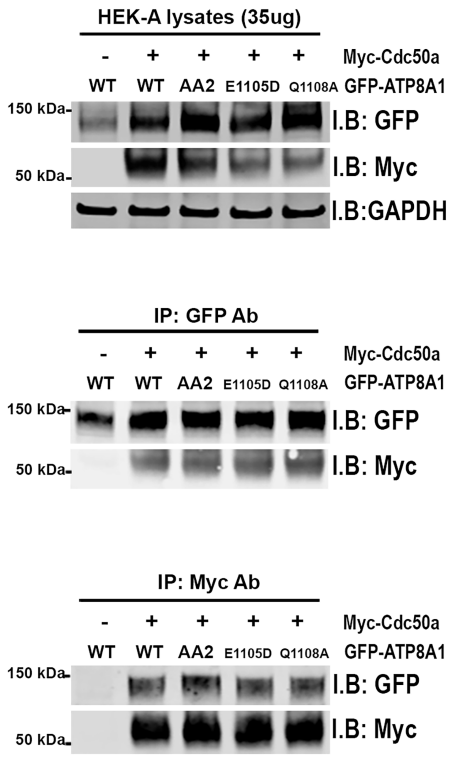

Figure S4. GFP-ATP8A1-E1105D and GFP-ATP8A1-Q1108A bind myc-CDC50A.

Protein expression and co-immunoprecipitation of mutagenized GFP-ATP8A1 in HEK cells. Immunoblotting of HEK lysates (35 μg per lane) is shown using anti-GFP antibody or anti-Myc antibody in the upper panel. Co-immunoprecipitation utilizing anti-GFP antibodies (middle panel) or anti-Myc antibodies (bottom panel) used 500 μg of input lysate (representative of 2 experiments).

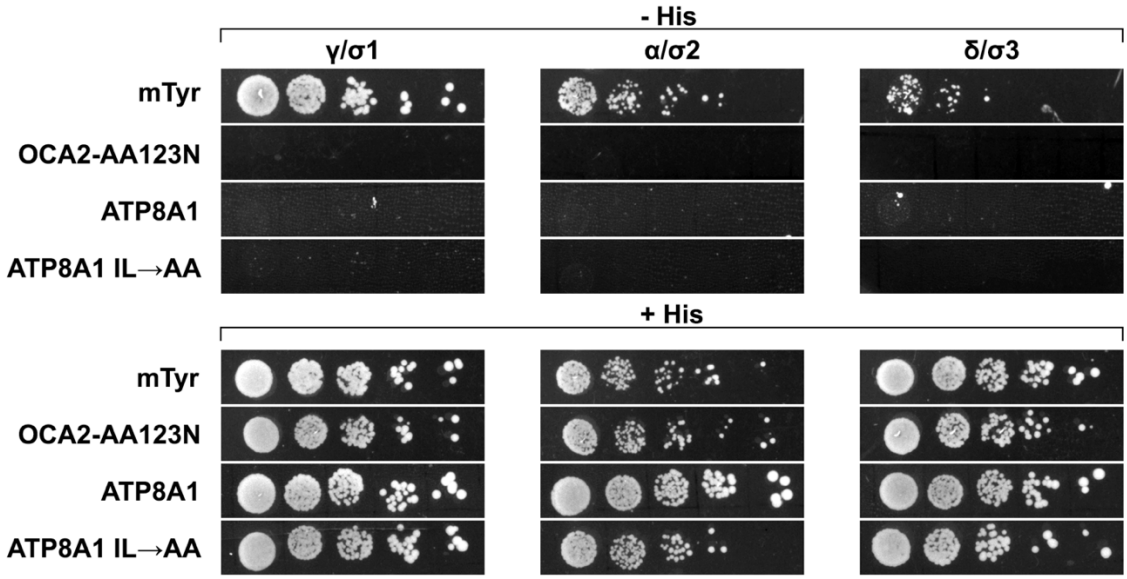

Figure S5: Yeast 3-hybrid assay to assess binding between the ^{1105}ERAQLL and AP-3.

To test whether the ^{1105}ERAQLL motif of ATP8A1 binds to AP-3, we employed a previously described, highly sensitive yeast 3-hybrid assay **(1)** in which the GAL4 transcription factor activation domain was fused to the γ, α or δ subunit of AP-1, -2, or -3 respectively and co-expressed in *cerevisiae* H57c cells with the corresponding s subunit (σ1 for AP-1, σ2 for AP-2 and σ3A for AP-3) and the GAL4 DNA binding domain (DBD) fused to the C-terminal cytoplasmic domain (residues 1071 to 1164) of human ATP8A1. Whereas the positive control – the Gal4 DBD fused to the cytoplasmic domain of mouse tyrosinase (mTyr) **(2, 3)** yielded a robust interaction as detected by growth of yeast on plates lacking histidine, neither the negative control (OCA2-AA123N;**(3)**) nor WT or dileucine mutant variants of the ATP8A1 cytoplasmic domain yielded a positive interaction.

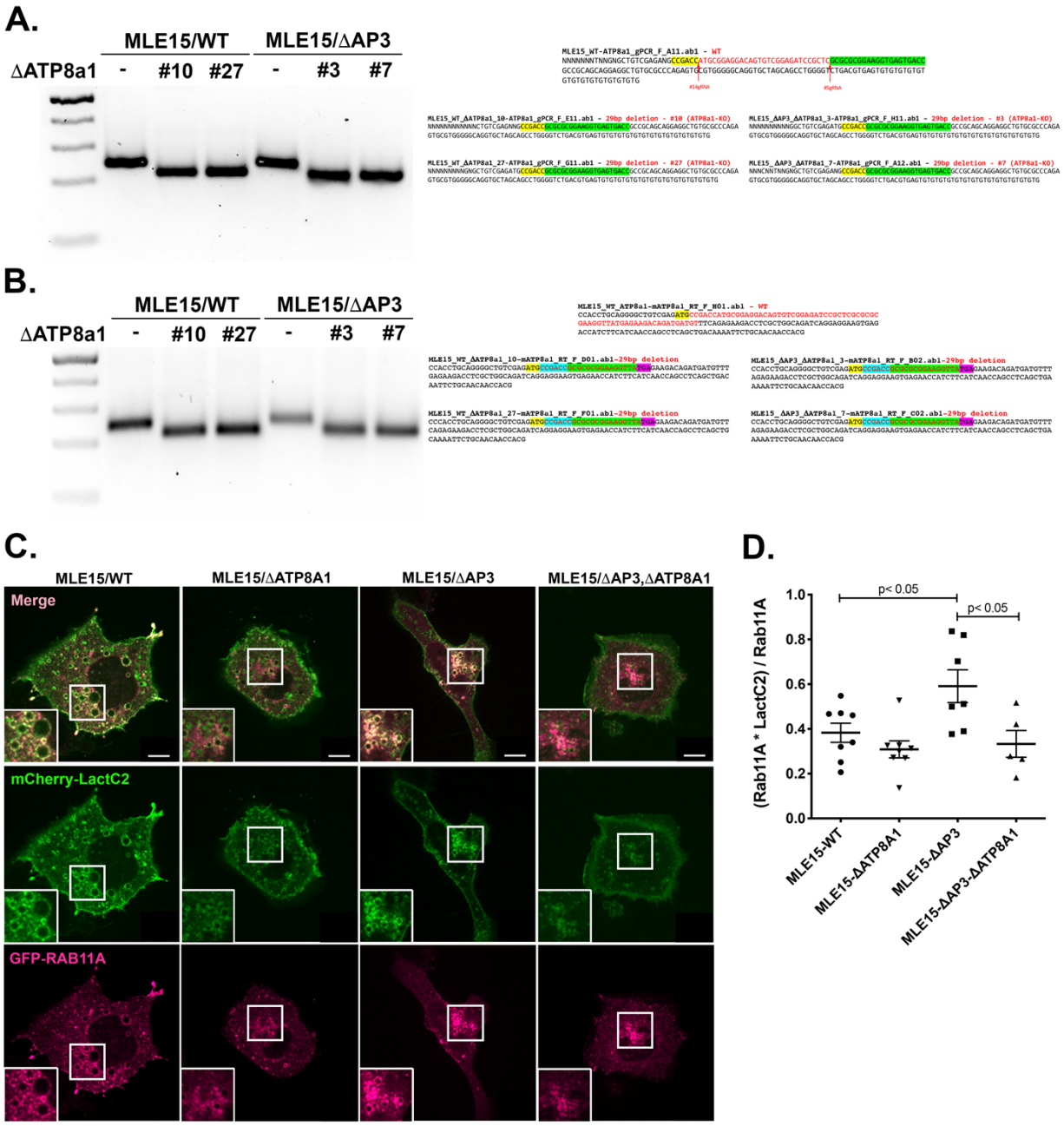

Figure S6: Endogenous ATP8A1 function in MLE15 cells enhances cytosolically exposed PtdSer at subcellular membranes.

A. CRISPR strategy for generating MLE15/WT-ΔATP8A1 and MLE15/ΔAP3-ΔATP8A1.
(A) Genomic PCR products and sequencing demonstrating the deletions induced by the double CRISPR-mediated Cas9 cleavages. Gel electrophoresis of genomic PCR products from MLE15/WT and MLE15/ΔAP3 starting cells, and two clones demonstrating successful deletions of 29 bp in exon 1 of *Atp8a1*.

B. RT-PCR products and sequencing demonstrating induced by the double CRISPR-mediated Cas9 cleavages expressed in *Atp8a1* RNA. Gel electrophoresis of genomic PCR products from MLE15/WT

and MLE15/ΔAP3 starting cells, and two clones demonstrating successful deletions of 29 bp in exon 1 of *Atp8a1*.

C. Live cell imaging of MLE15/WT, MLE15/ΔAP3, MLE15/ΔATP8A1, and MLE15/ΔAP3-ΔATP8A1 cells. Representative pseudocolor images captured from live cell imaging of MLE15/WT, MLE15/ΔAP3, MLE15/ΔATP8A1, and MLE15/ΔAP3-ΔATP8A1 cells expressing the biosensor mCherry-LactC2 (pseudocolor Green) and GFP-Rab11A (pseudocolor Magenta; scale bars = 10 microns). Live cell imaging was obtained using identical microscope settings, and still images were derived from the first frame to avoid photobleaching.

D. Colocalization correlation between GFP-RAB11A (pseudocolor Magenta) and mCherry-LactC2 (pseudocolor Green) acquired from images described in S6C (n=5-8 cells per group, mean ± standard error). The method used for colocalization was adapted from Dennis et al (4) (see Methods).

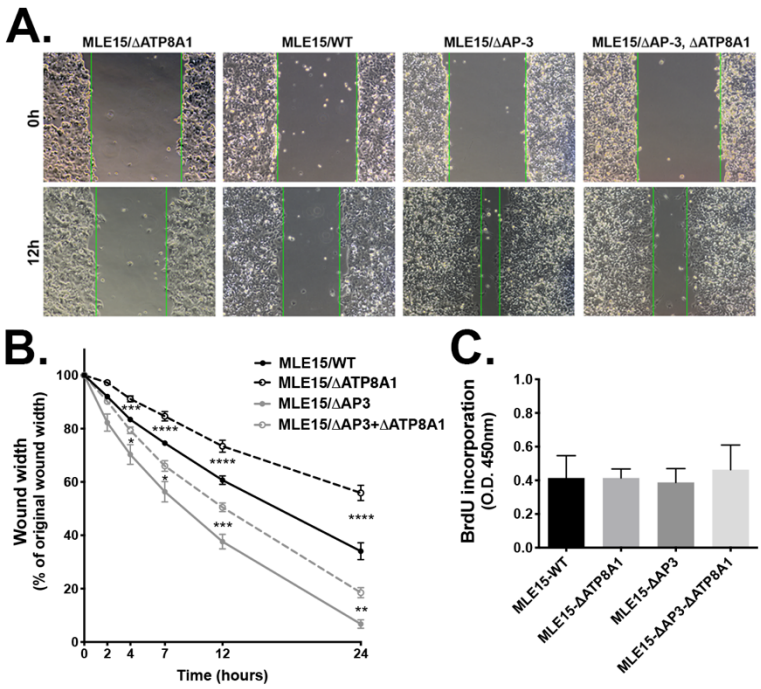

Figure S7: Activation of YAP in MLE15/ΔAP3 cells hastens scratch wound healing in an ATP8A1-dependent manner.

A. Composite of phase contrast images depicting scratch wound of confluent monolayer of MLE15/ΔATP8A1, MLE15/WT, MLE15/ΔAP3, and MLE15/ΔAP3-ΔATP8A1 cells immediately post-wounding and 12 h after wounding.

B. Time course of wound closure after scratch wounding (see Methods). MLE15/WT cells ± ATP8A1 and MLE15/ΔAP3 cells ± ATP8A1 were monitored over 24h as they closed the wound depicted in panel A. MLE15/ΔAP3 cells closed a scratch wound faster than MLE15/WT cells (1h $p<.05$, 2-4h $p<.001$, and 7-24h $p<.0001$; asterisks not provided on graph). Loss of ATP8A1 slowed closure in both MLE15/WT and MLE15/ΔAP3 cells (n= 3 experiments with triplicate samples at each timepoint; *$p<.05$, **$p<.01$, ***$p<.001$ with the asterisks placed between the MLE15/WT and MLE15/ΔATP8A1, or MLE15/ΔAP3 and MLE15/ΔAP3-ΔATP8A1 cells, respectively).

C. Proliferation of MLE15/WT, MLE15/ΔAP3, MLE15/ΔATP8A1, and MLE15/ΔAP3-ΔATP8A1 cells as measured by BrdU incorporation (see Methods) over 8 h. No significant differences were detected (n = 2 experiments performed with quadruplicate samples).

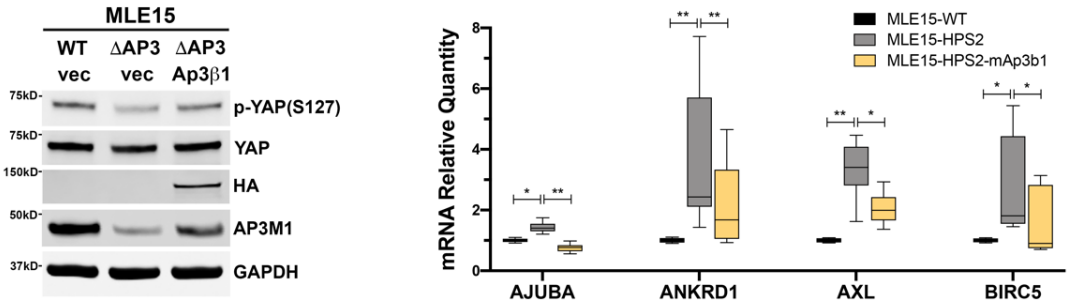

Figure S8: Rescue of YAP activation by restoring AP-3 in MLE15/ΔAP3 cells.

Left panel: Composite representative immunoblot from MLE15/WT and MLE15/ΔAP3 cells expressing from empty vector, and MLE15/ΔAP3 cells expressing *Ap3b1*-HA, as described in Figure 2 (representative of 3 biologic comparisons).

Right panel: RT-qPCR for *Ajuba, Ankrd1, Axl, Birc5* RNA (n= triplicate samples of 3 biologic replicates; n=3; box and whiskers plot as described in Figure 7A; *p < .05, **p < .01, ***p < .001, ****p < .0001).

Supplemental Tables

Table S1: gRNA sequences used for inactivating *Ap1g1* and *Atp8a1*.

Target Gene	gRNA name	gRNA Sequence (5'→3')	Genomic PCR primers (5'→3')	
Ap1γ1	Ap1γ1-gRNA#3	CACCGATCACTGTAAGAGAAAAAG	Forward	GAAACTTTGTTAGGCTGCTTCG
	Ap1 γ 1-gRNA#5	CACCGTGCAGAGATCTTGCGGGAG	Reverse	CTTTCAAAAATAAGTGCCCTGG
ATP8a1	ATP8a1-gRNA#5	CACCGACTCACCTTCCGCGCGCGAG	Forward	GTGACAGGTGCAGGGTCC
	ATP8a1-gRNA#14	CACCGCTGTCGAGATGCCGACCATG	Reverse	GGTGTAGATGGGATGAGGTGTC

Table S2: Primers used to construct *Atp8a1* mutations of dileucine motifs.

Mutant	1st PCR				2nd PCR	
	5' fragment		3' fragment			
AA1	F	TACACTGGACATGACACCAAG	F	CAGGAAGAAAGATATGAAGCGGCCAATGTCTTGGAGTTTACC	F	TACACTGGACATGACACCAAG
	R	GGTAAACTCCAAGACATTGGCCGCTTCATATCTTTCTTCCTG	R	ATTAGCTGCCTGCAGGCCTTCATT	R	ATTAGCTGCCTGCAGGCCTTCATT
AA2	F	AATGAAGGCCTGCAGGCAGCTAAT	F	CTGACCGAGAGGGCGCAAGCGGCCAAGAACGTCTTTAAGAAG	F	AATGAAGGCCTGCAGGCAGCTAAT
	R	CTTCTTAAAGACGTTCTTGGCCGCTTGCGCCCTCTCGGACAG	R	GCGGATCCCGGGTCACCATTC	R	GCGGATCCCGGGTCACCATTC
E1105D	F	AATGAAGGCCTGCAGGCAGCTAAT	F	GGAAAAAGCCTGACCGACAGGGCGCAACTGCTCAAG	F	AATGAAGGCCTGCAGGCAGCTAAT
	R	CTTGAGCAGTTGCGCCCTGTCGGTCAGGCTTTTTCC	R	GCGGATCCCGGGTCACCATTC	R	GCGGATCCCGGGTCACCATTC
Q1108A	F	AATGAAGGCCTGCAGGCAGCTAAT	F	CTGACCGAGAGGGCGGCACTGCTCAAGAACGTCTTT	F	AATGAAGGCCTGCAGGCAGCTAAT
	R	AAAGACGTTCTTGAGCAGTGCCGCCCTCTCGGTCAG	R	GCGGATCCCGGGTCACCATTC	R	GCGGATCCCGGGTCACCATTC

Supplemental Videos

Supplemental Videos SV1-SV4: Live cell imaging MLE15/WT (SV1), MLE15/ΔAP3 (SV2), MLE15/ΔATP8A1 (SV3), and MLE15/ΔAP3-ΔATP8A1 (SV4) cells expressing mCherry-ABCA3 and the biosensor GFP-LactC2 used to generate still images in Figure 7.

Supplemental Videos SV5-SV8: Live cell imaging MLE15/WT (SV5), MLE15/ΔAP3 (SV6), MLE15/ΔATP8A1 (SV7), and MLE15/ΔAP3-ΔATP8A1 (SV8) cells expressing GFP-RAB11 (pseudocolored Magenta) and the biosensor mCherry-LactC2 (pseudocolored Green) used to generate still images in Supplemental Figure 6.

SI References

1. K. Janvier, *et al.*, Recognition of dileucine-based sorting signals from HIV-1 Nef and LIMP-II by the AP-1 γ–σ1 and AP-3 δ–σ3 hemicomplexes. *J Cell Biology* **163**, 1281–1290 (2003).

2. A. C. Theos, *et al.*, Functions of Adaptor Protein (AP)-3 and AP-1 in Tyrosinase Sorting from Endosomes to Melanosomes. *Mol Biol Cell* **16**, 5356–5372 (2005).

3. A. Sitaram, *et al.*, Differential recognition of a dileucine-based sorting signal by AP-1 and AP-3 reveals a requirement for both BLOC-1 and AP-3 in delivery of OCA2 to melanosomes. *Mol Biol Cell* **23**, 3178–3192 (2012).

4. M. K. Dennis, *et al.*, BLOC-2 targets recycling endosomal tubules to melanosomes for cargo delivery. *J Cell Biology* **209**, 563 577 (2015).